Supplement of Atmos. Chem. Phys., 23, 15135–15147, 2023
https://doi.org/10.5194/acp-23-15135-2023-supplement

Atmospheric Chemistry and Physics Open Access

Supplement of

Direct formation of HONO through aqueous-phase photolysis of organic nitrates

Juan Miguel Gonzá

Correspondence to: Juan Miguel González-Sánchez (juangonzalez.sc@proton.me) and Anne Monod (anne.monod@univ-amu.fr)

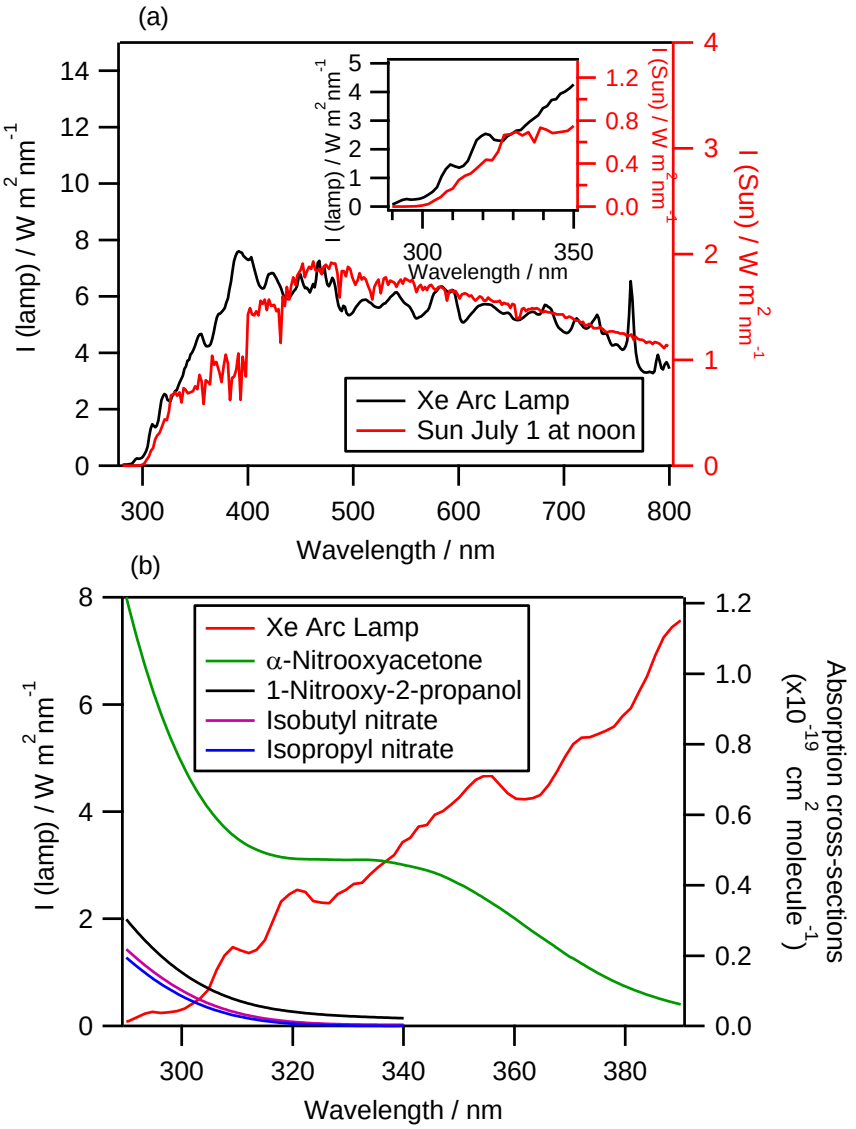

Figure S1: (a) Irradiation spectra of the Xe 1000 W arc lamp equipped with an AM1.5 filter (black line) compared to the solar irradiation spectra (red line) on the 1st of July 2015 at 40° latitude at ground level with an overhead ozone column of 300 DU and a surface albedo of 0.1 (using the Tropospheric Ultraviolet (TUV) model, Madronich and Flocke, 1999**). Inner graph: zoom on the 290 to 350 nm region. (b) Absorption cross-sections of the investigated $RONO_2$ in methanol and/or water: α-nitrooxyacetone (green), 1-nitrooxy-2-propanol (black), isobutyl nitrate (violet), and isopropyl nitrate (blue), compared to the Xe lamp irradiation spectra (red).**

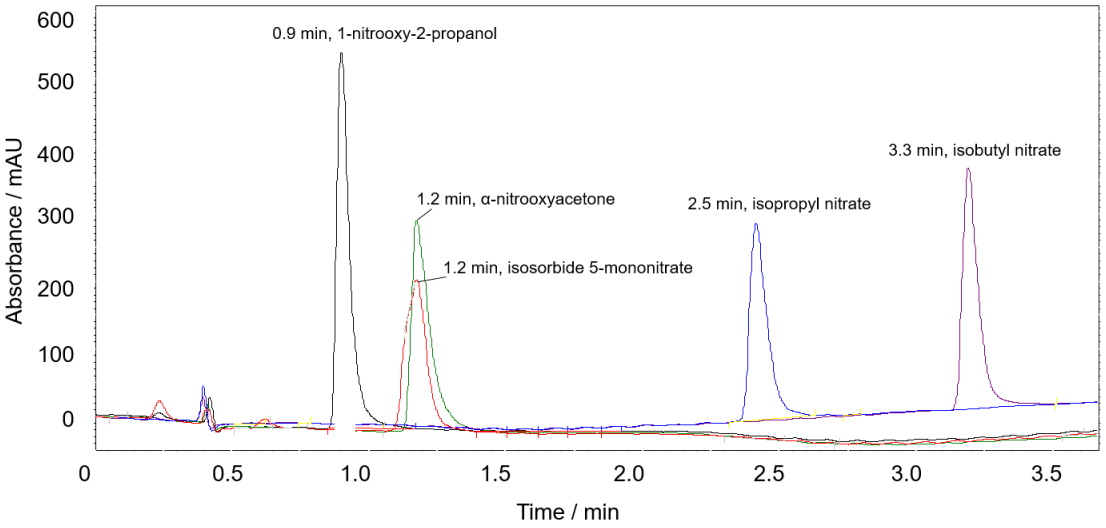

Figure S2: UHPLC-UV chromatograms of 1-nitrooxy-2-propanol (black), isosorbide 5-mononitrate (red), α-nitrooxyacetone (green), isopropyl nitrate (blue), and isobutyl nitrate (violet) at 200 nm. All compounds were injected at 3 ·10^{-4} mol L^{-1}.

Section S1: Analytical performances of GC-MS analysis of $RONO_2$

GC-MS retention times and fragmentation patterns were investigated for isopropyl nitrate, isobutyl nitrate, α-nitrooxyacetone, 1-nitrooxy-2-propanol, isopentyl nitrate, 1-pentyl nitrate, and isosorbide 5-mononitrate. Their retention times were 6.0, 7.1, 12.3, 12.4, 13.0, 14.0, 20.5 min, respectively. Note that isopropyl nitrate showed a retention time lower than time when the EI filament was turned on (at 7 min). For this compound, headspace analysis of a sample containing pure isopropyl nitrate were performed to prevent from saturating the source with any solvent. Figure S1.1 shows the GC-MS chromatographic peaks of isobutyl nitrate, isopentyl nitrate, 1-pentyl nitrate, and isosorbide 5-mononitrate. The intensity of the chromatographic peaks is very sensitive to the volatility of the $RONO_2$ (i.e., significant amounts of isobutyl nitrate are lost during the sample preconcentration step), its polarity (i.e., only ~ 24 % of isosorbide 5-mononitrate is extracted during the CH_2Cl_2 extraction step) and its ionization efficiency. This complicates the quantification of these compounds. Nevertheless, $RONO_2$ can be detected at very low concentrations.

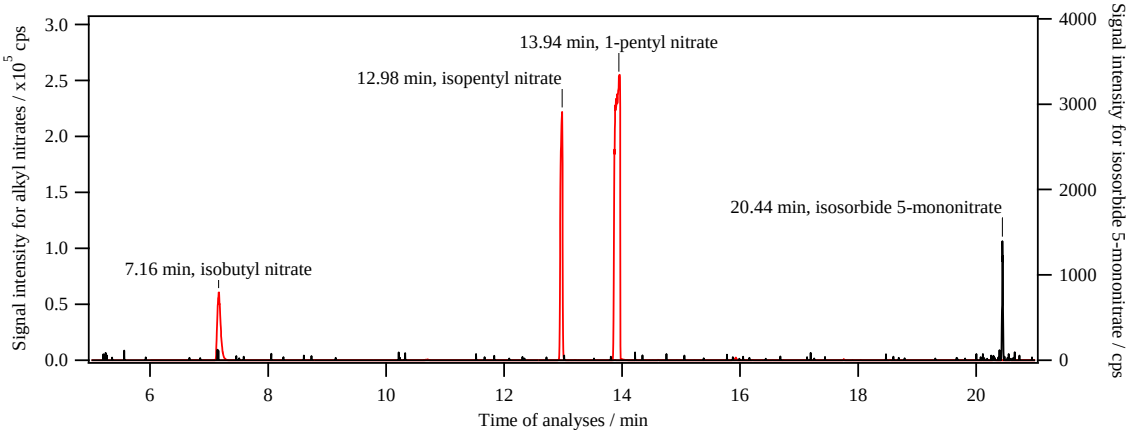

Figure S1.1: Gas chromatogram for isobutyl nitrate, isopentyl nitrate, 1-pentyl nitrate, and isosorbide 5-mononitrate. The compounds were extracted using the developed protocol (Section 2.3.3) from solutions containing 0.05 mM for alkyl nitrates, and 0.01 mM for isosorbide 5-mononitrates. The m/z = 46 fragment (NO_2^+) is extracted in each chromatogram.

Figure S1.2 shows their mass spectra. All compounds present highly fragmented mass spectra, and the molecular ion $RONO_2^+$ was not observed. In all analyses, the m/z = 46, corresponding to the ion NO_2^+, was obtained, thus validating the methodology of extracting the mass-to-charge ratio 46 to identify $RONO_2$ compounds in the "end of reaction" solutions (Section 2.2). The m/z = 46 fragment can also be observed for nitro compounds or peroxynitrates. Peroxynitrates might be formed, however, these compounds are thermally unstable and thus, likely decompose during their injection or elution in GC-MS analyses.

Figure S1.3 shows that the smallest molecules (i.e., isopropyl nitrate, isobutyl nitrate, α-nitrooxyacetone, and 1-nitrooxy-2-propanol) present clear fragmentation patterns. For all compounds, the R^+ fragment was observed: $CH_3CHCH_3^+$, $CH_3CH(CH_3)CH_2^+$, $CH_3COCH_2^+$ and $CH_3CH_2(OH)CH_2^+$ at m/z = 43, m/z = 57, m/z = 57 and m/z = 59 for isopropyl nitrate, isobutyl nitrate, α-nitrooxyacetone and 1-nitrooxy-2-propanol, respectively. Fragmentation of the R^+ was also observed for the three latter ions providing the most intense peaks: $CH_3CHCH_3^+$ for isobutyl nitrate (m/z = 43), CH_3CO^+ for α-nitrooxyacetone (m/z = 43) and $CH_3CH_2(OH)^+$ for 1-nitrooxy-2-propanol (m/z = 45). For all primary nitrates, m/z = 76 was detected, corresponding to $CH_2ONO_2^+$ ion, while isopropyl nitrate showed the $CH_3CHONO_2^+$ fragment, observed at m/z = 90.

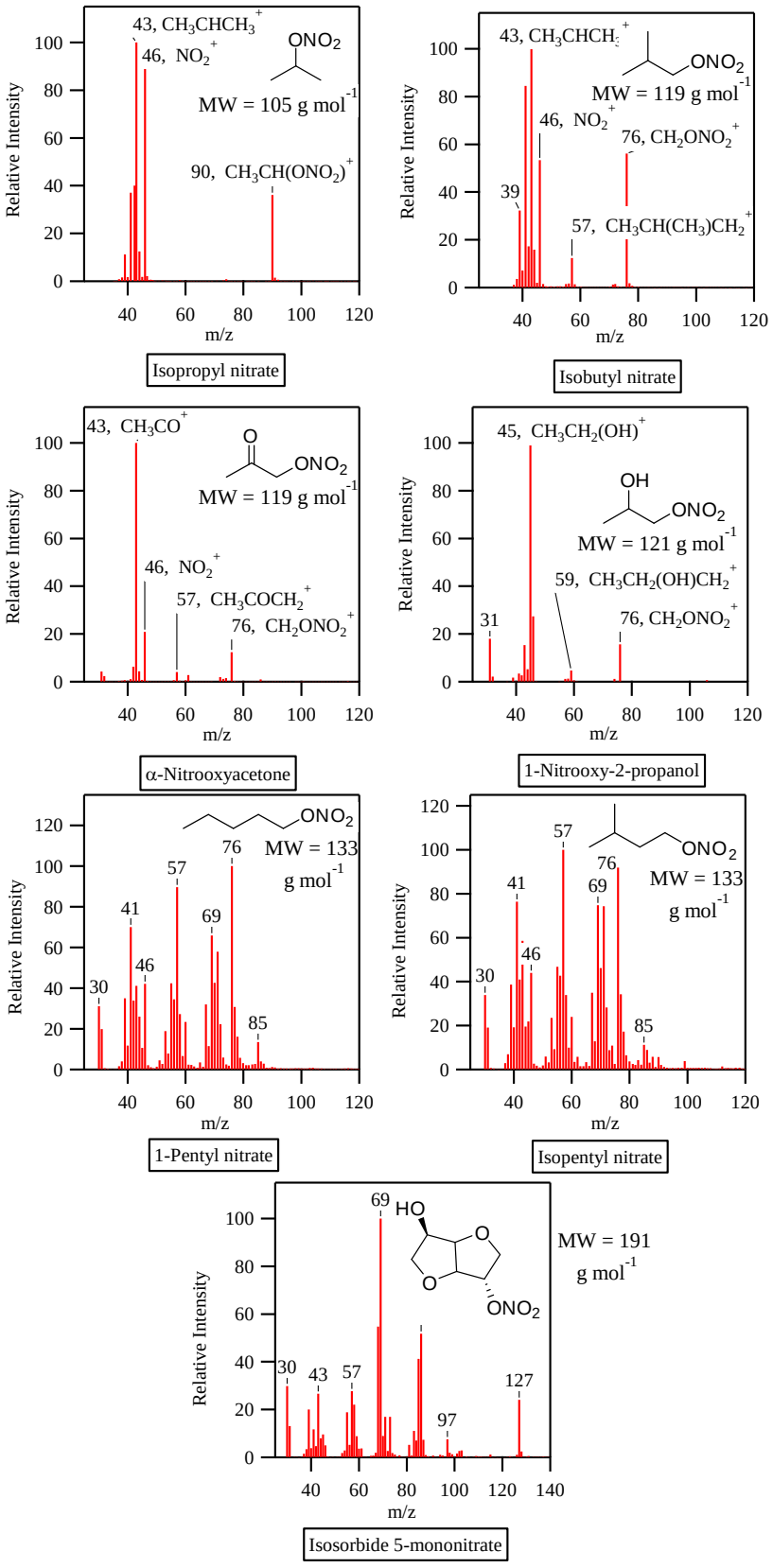

Figure S1.2: Mass spectra analyzed by GC-MS for the standard and synthesized $RONO_2$.

For 1-pentyl nitrate, isopentyl nitrate, and isosorbide 5-mononitrate much more fragmentations were observed. Due to their similar structure, the same peaks were detected for 1-pentyl nitrate and isopentyl nitrate, with only

small changes in their relative intensities. The R^+ fragment was detected at m/z = 71, as well for the $CH_2ONO_2^+$ fragment (m/z = 76). Other fragments such as $C_3H_7^+$ and $C_4H_9^+$ were also detected at m/z = 43 and m/z = 57, respectively. For isosorbide 5-mononitrate, the detected m/z = 127, probably corresponds to the fragment obtained once NO_2 and a water molecule are lost. The most intense peak at m/z = 69, likely corresponds to a furane-unit.

In any case, the fragmentation observed for these $RONO_2$ offers precious informations for elucidating the structures of the detected molecules during isopropyl nitrate and isobutyl nitrate photolysis.

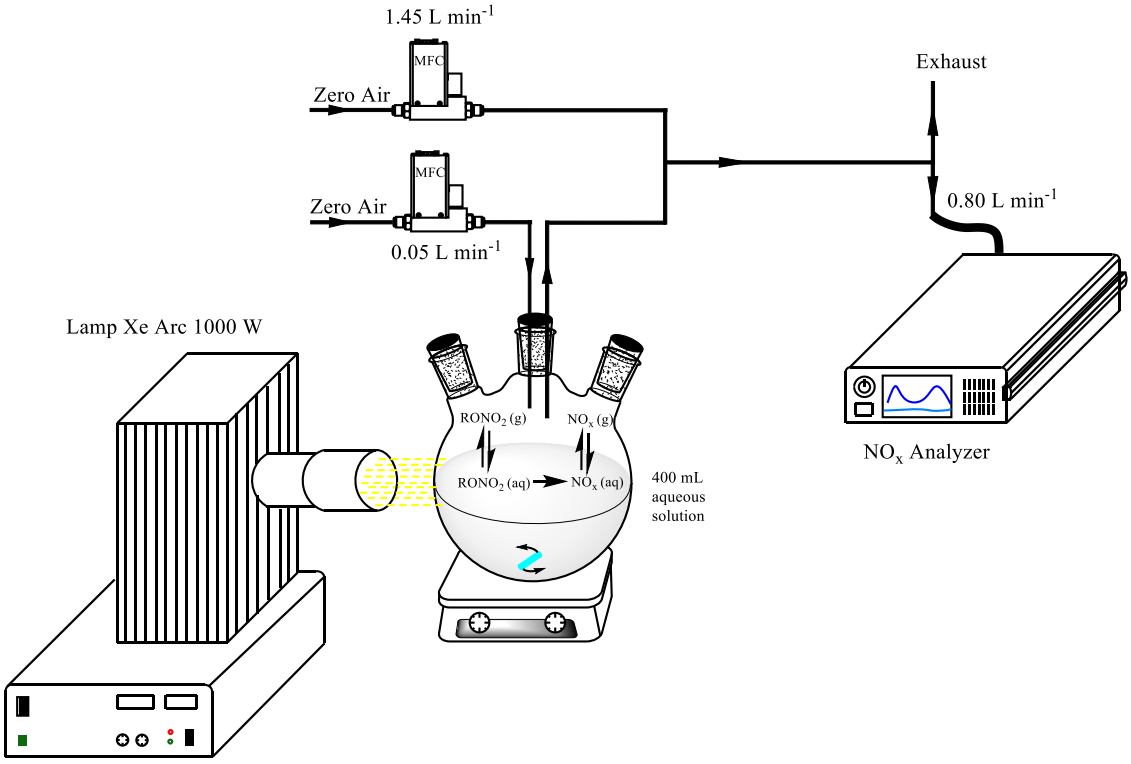

Figure S3: Experimental setup used for the detection of $\cdot NO_{(g)}$ and $\cdot NO_{2(g)}$ in the reactor's headspace during the aqueous-phase reactivity of $RONO_2$.

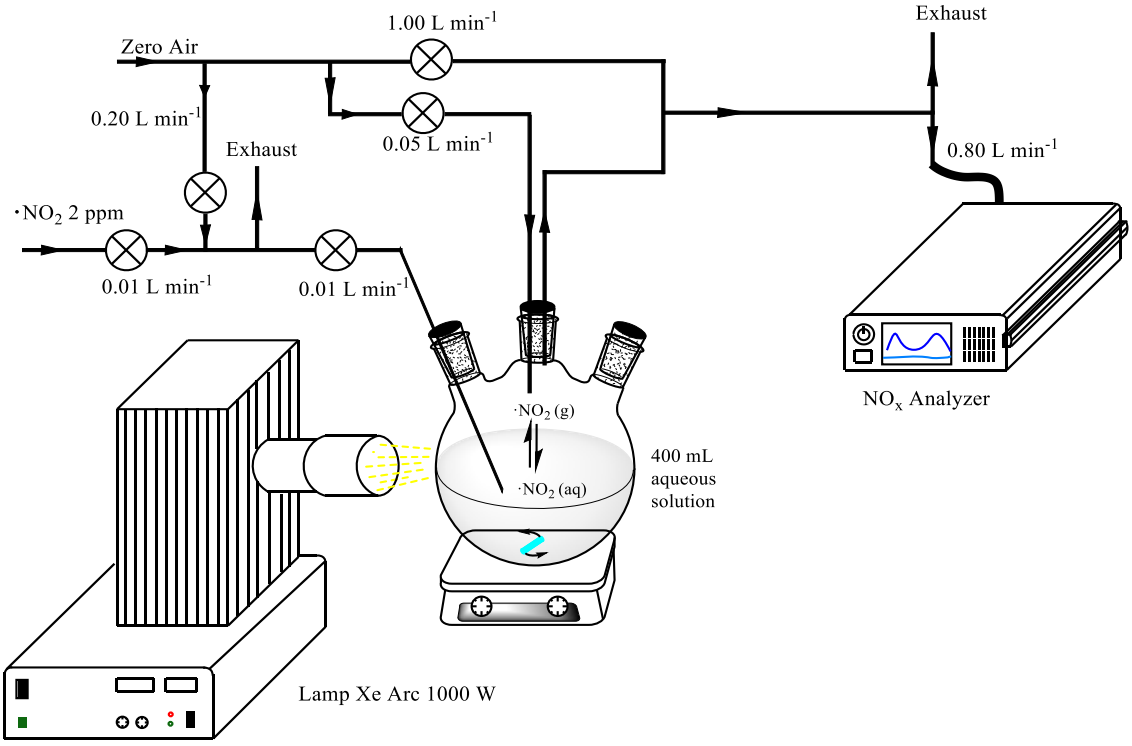

Figure S4: Experimental setup used for the NO_x control experiment: $\cdot NO_{2(g)}$ was bubbled in the reactor's aqueous phase and then photolyzed by exposing it to the lamplight.

Section S2: Interferences of $RONO_2$ in the NO_x Analyzer

The CLD 88p Ecophysics measurements are based on the following principles. Ozone is generated photochemically and used to oxidize ·NO to the excited form of $·NO_2$ ($·NO_2$*). The latter can undergo photochemical relaxation emitting light with a maximum at 1200 nm. The light emitted is proportional to the ·NO concentration and is detected by photomultiplicators. Repeatedly, the sampled air is guided to a photolytic commercial converter (PCL 860 Ecophysics) where $·NO_2$ is converted to ·NO by photolysis at 320 – 400 nm. The total ·NO is measured to obtain the NO_x concentration and $·NO_2$ concentration is obtained by subtraction.

In our experiments, interferences with the $RONO_2$ were observed. During the first 30 min of Experiment 1 (before photolysis, Table 1), an increase in the $·NO_2$ signal was observed immediately after the injection of isopropyl nitrate into the reactor's aqueous phase (Fig. S2.1). The signal stabilized at ~110 ppbv. Since no reactivity occurred at that moment, the signal was only generated by the conversion of isopropyl nitrate partitioned into the reactor's headspace, into ·NO in the photolytic converter. The concentration of isopropyl nitrate in the reactor's headspace was estimated to be ~1300 ppmv (considering its aqueous-phase concentration and K_H value). Therefore, the conversion of $RONO_2$ to ·NO is very low in good agreement with the fact that the photolytic converter filters light out of the 320 to 400 nm range to minimize interferences due to NO_y species and provoke interferences lower than 0.6 % (Ryerson et al., 2000).

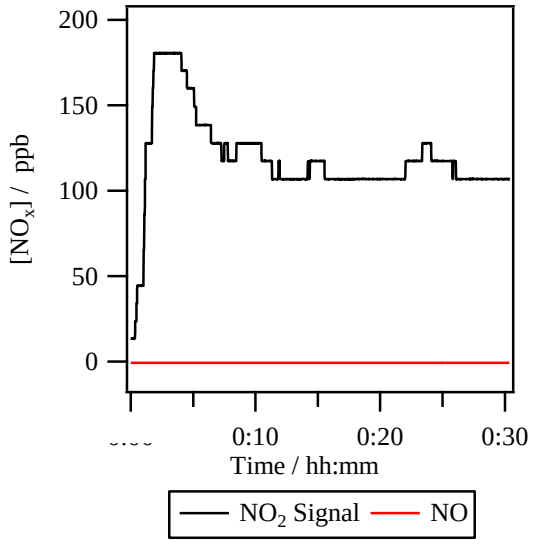

Figure S2.1: ·NO and $·NO_2$ signal time profiles in the first 30 minutes of Exp. 1 when isopropyl nitrate (1 mM) is injected into the aqueous phase of the photoreactor, before photolysis.

Section S3: Classical dynamics of isopropyl nitrate in water

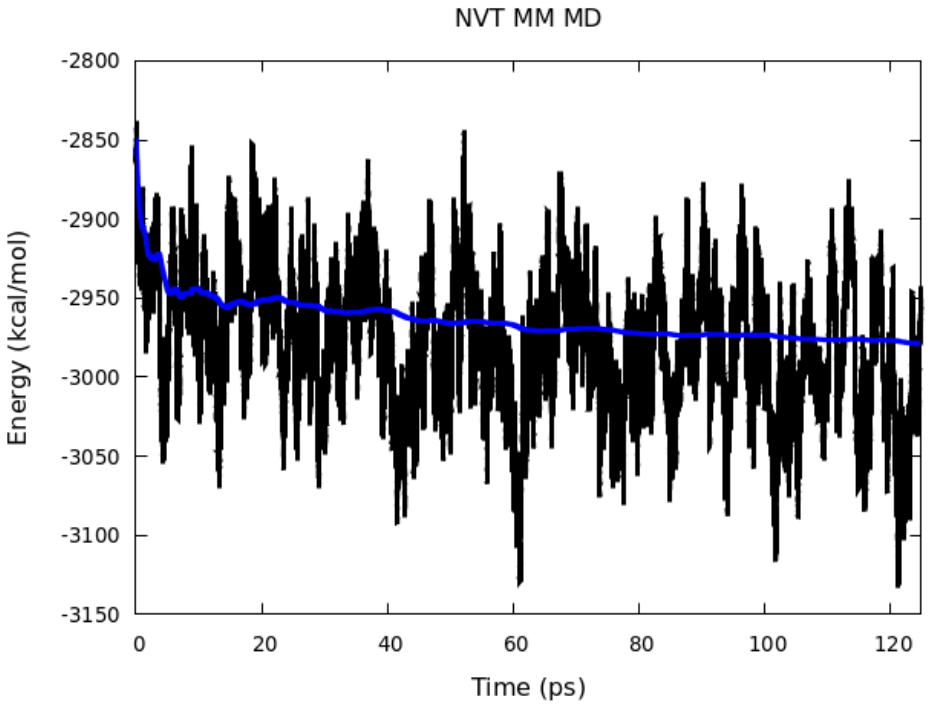

Figure S3.1: MD dynamics for 125 ps (1 fs timestep) in an NVT ensemble at fixed isopropyl nitrate (black: energy value, blue: running average).

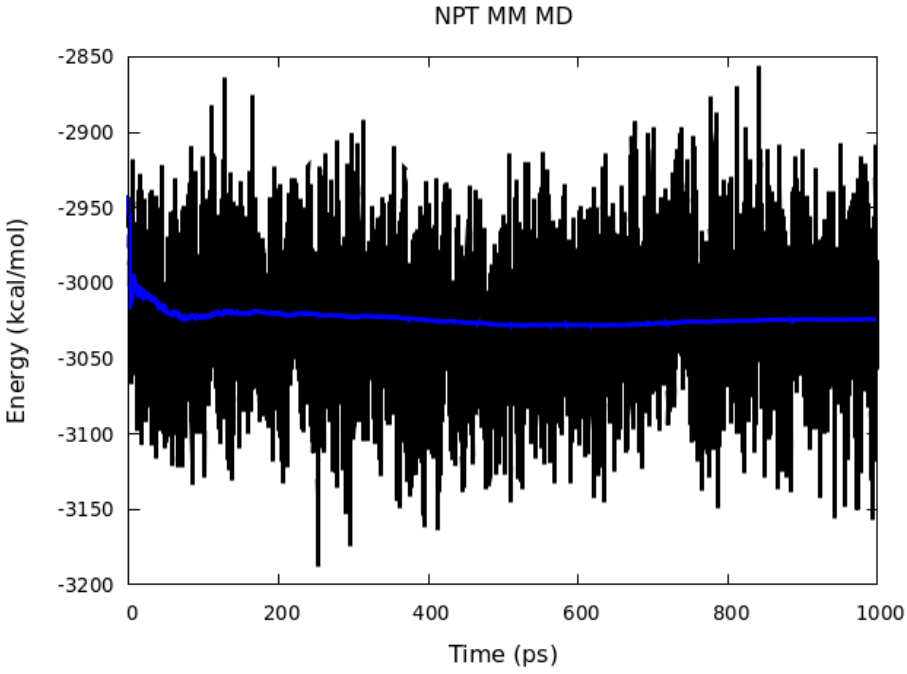

Figure S3.2: MD dynamics for 1 ns (1 fs timestep) in an NPT ensemble at fixed isopropyl nitrate (black: energy value, blue: running average).

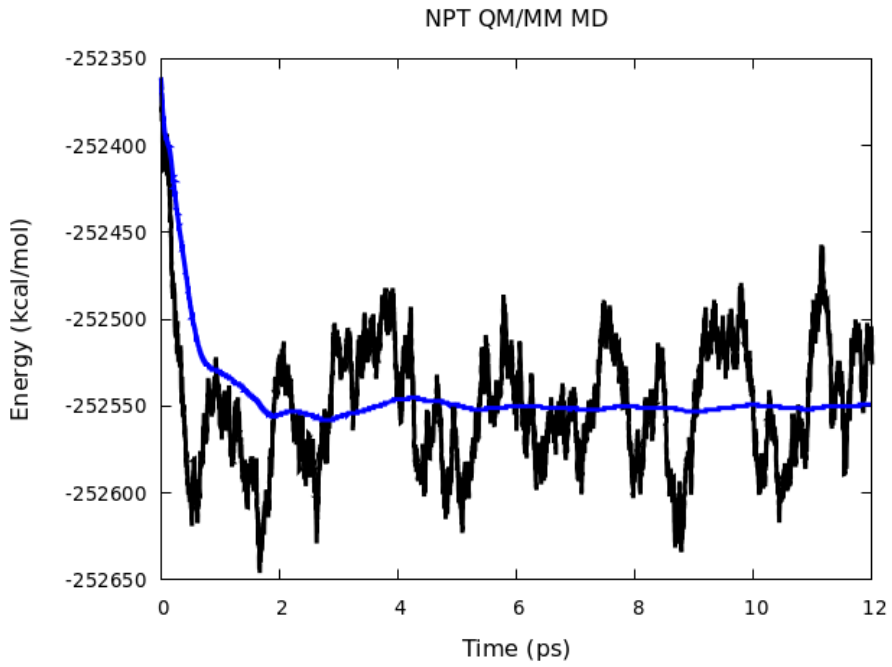

Figure S3.3: B3LYP/6-31G*//Amber99 MD dynamics for 12 ps (1 fs timestep) in an NPT ensemble relaxing the full system (black: energy value, blue: running average).

Table S1: Initial conditions and yields of primary reaction products during the photolysis experiments. (sec. = secondary reaction products)

Exp	$RONO_2$	$[RONO_2]_0$ (mM)	Decay ($\cdot 10^{-5}$ s^{-1})	% cosumed at end	HNO_2	HNO_3	Isobutyral-dehyde (%)	Acetone (%)	Hydroxy-acetone (%)	Lactal-dehyde (%)	Acetal-dehyde (%)	Formal-dehyde (%)	Acetic acid (%)	Formic acid (%)	IP3	IB1	IB2
2	Isopropyl nitrate	0.93	1.9	38	40	sec.		32			5		sec.	sec.	sec.		
3	Isopropyl nitrate	1.81	1.4	29				88	3		5	sec.			sec.		
4	Isopropyl nitrate	1.71	1.0	17	59	sec.		74	4		5		sec.	sec.	sec.		
5	Isobutyl nitrate	0.60	2.9	52												sec.	sec.
6	Isobutyl nitrate	0.59	2.5	47												sec.	sec.
7	Isobutyl nitrate	0.53	1.9	38												sec.	sec.
8	Isobutyl nitrate	0.55	2.6	48	31	sec.	5	20				39				sec.	sec.
9	Isobutyl nitrate	0.49	1.4	30			4	32				37					
10	α-Nitrooxyacetone	1.18	0.7	16	>28	sec.			sec.		sec.	79		96			
11	1-Nitrooxy-2-propanol	0.72	0.6	15	62	sec.				14	70	71	sec.	sec.			
12	1-Nitrooxy-2-propanol	0.38	0.7	16	59	sec.				8	50	63	sec.	sec.			

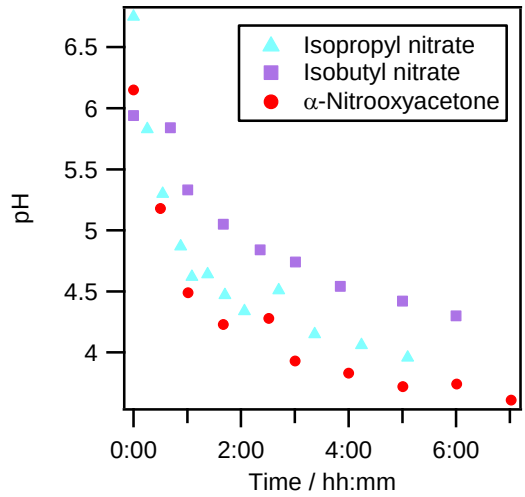

Figure S5: pH time profiles during the photolysis of isopropyl nitrate (Exp. 2), isobutyl nitrate (Exp. 8), and α-nitrooxyacetone (Exp. 10).

Section S4: Observation of acetic acid and methyglyoxal formation during α-nitrooxyacetone aqueous-phase photolysis

As both lactate and acetate anions present very similar retention times in our analyses (5.7 vs 6.0 min), the occurrence of a large peak due to the lactate anion rendered impossible the quantification of the acetate carboxylate although the latter was identified as a significant reaction product (Fig. S4.1).

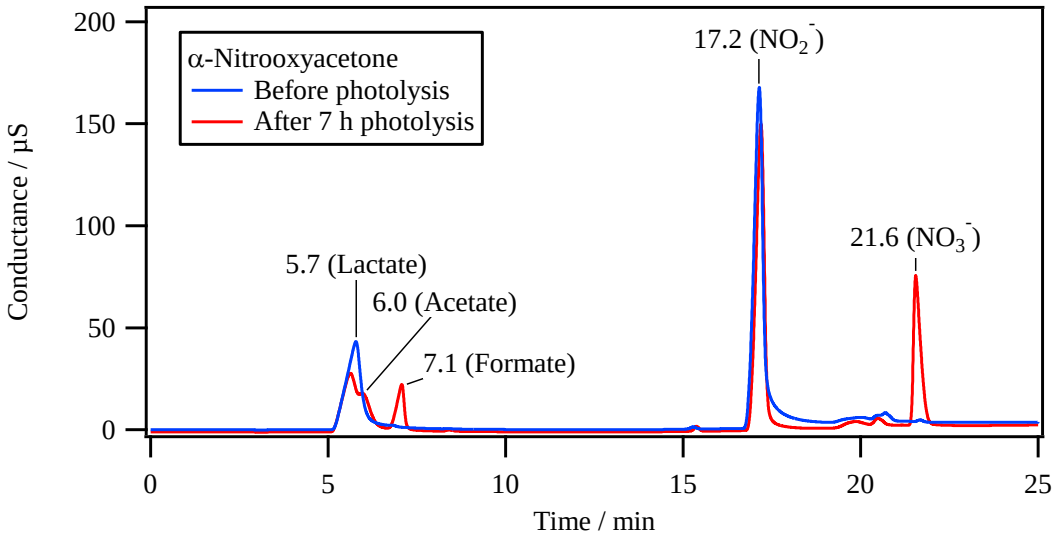

Figure S4.1: α-Nitrooxyacetone photolysis reaction products: ionic chromatogram of α-nitrooxyacetone in water before photolysis (blue) and after 7 h of photolysis (red). (Exp 10 in Table S1).

The quantification of methylglyoxal by DNPH derivatization and UHPLC-UV was impeded by oligomerization reactions (Fig. S4.2). The acidic conditions needed for the derivatization reaction with 1,4-DNPH provoked aldol condensation reactions of methylglyoxal. This reaction was observed on a solution containing 10^{-4} M of methylglyoxal and resulted in an unresolved broad peak at the end of the UHPLC-UV chromatogram (7 to 9 min in Fig. S4.2). This hump was also observed during α-nitrooxyacetone photolysis, and thus the formation of methylglyoxal was confirmed after 100 min of photolysis, but it could not be quantified.

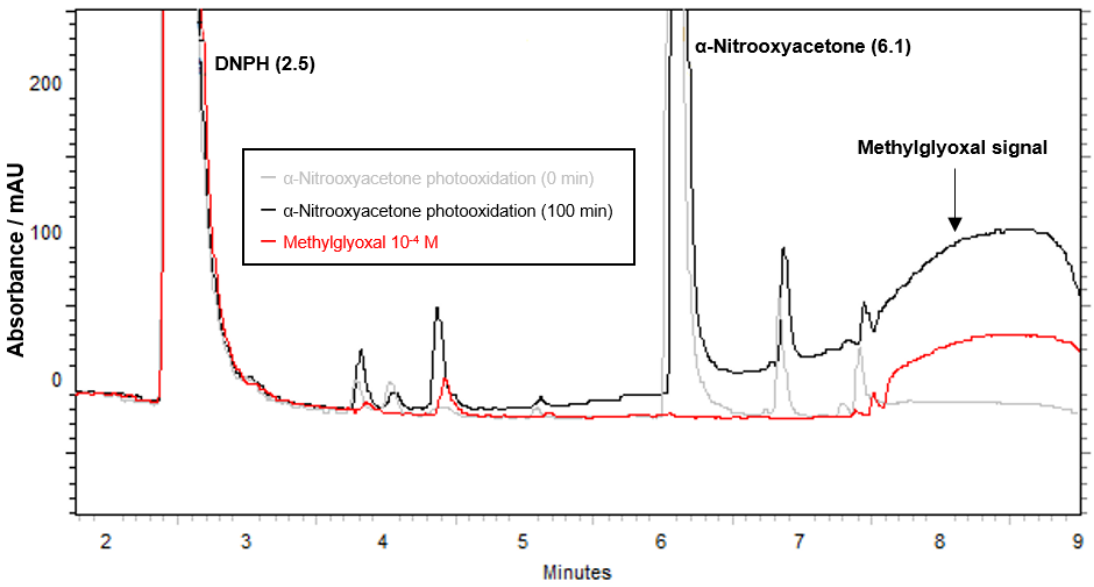

Figure S4.2: α-Nitrooxyacetone photolysis reaction products: UHPLC-UV chromatograms of DNPH-derivatized samples at time 0 and 100 min of photolysis (Exp 10 in Table S1), compared to a solution of methylglyoxal (10^{-4} M) at 360 nm.

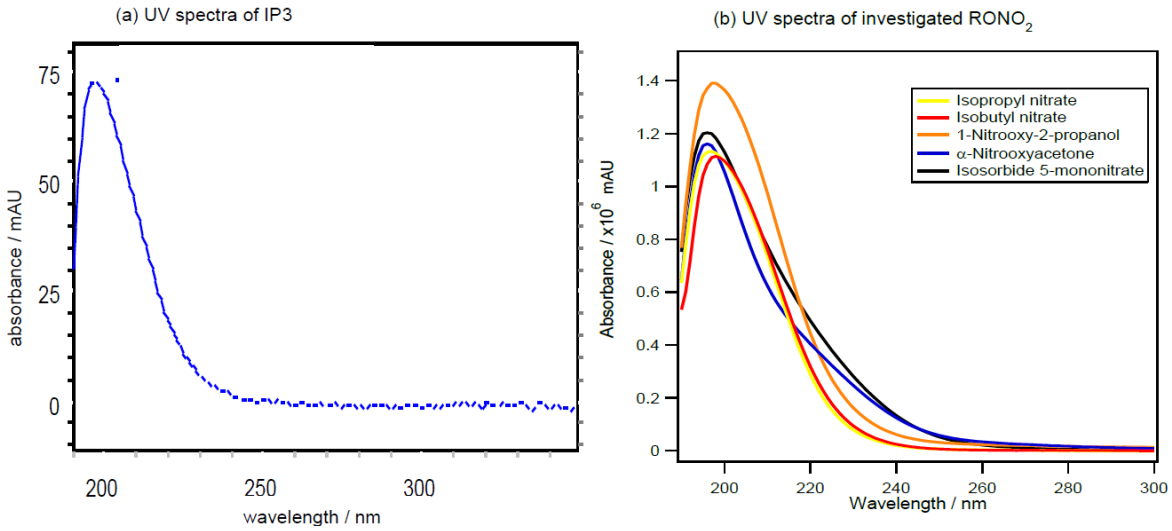

Figure S6: UV absorbance spectra obtained from the UHPLC-UV analyses: (a) IP3 (observed in Exp 2) and (b) standards of $RONO_2$ at ~10^{-3} M.

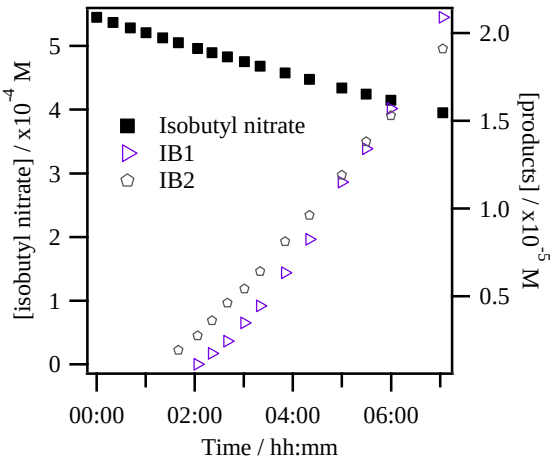

Figure S7: Isobutyl nitrate photolysis: time profiles of oxidized $RONO_2$ detected by non-derivatized UHPLC-UV analyses (Exp. 8 in Table S2).

Section S5: GC-MS analyses of the "end of reaction" for isobutyl nitrate and 1-nitrooxy-2-propanol

Figure S5.1a shows the chromatogram of the "end of reaction" (after 7 h of photolysis) for isobutyl nitrate. Up to nine chromatographic peaks corresponding to oxidized $RONO_2$ were detected at significant intensities (> $2 \cdot 10^5$ cps), the peak at 7.1 min corresponds to isobutyl nitrate. The obtained mass spectra (Fig. S5.1b) confirmed chemical structures corresponding to $RONO_2$ with similarities with isobutyl nitrate mass spectra (i.e., $C_3H_7^+$, $C_4H_9^+$ $CH_2ONO_2^+$ fragments at m/z = 43, 57, and 76, respectively). Functionalization of the organic chain was demonstrated by the presence of multiple fragmentations, and retention times higher than that of isobutyl nitrate. The mass spectra of IB6 and its retention time were identical to IP3, which was assigned to 1,2-propyl dinitrate. Further identification of IB7 and IB8 was performed upon the interpretation of the mass spectra. Nevertheless, the lack of standards prevented more precise identification.

For 1-nitrooxy-2-propanol, GC-MS analyses of the "end of reaction" confirmed the formation of $RONO_2$ although much fewer compounds were determined than during isopropyl nitrate and isobutyl nitrate photolysis (Figure S5.2). Four oxidized $RONO_2$ were observed including α-nitrooxyacetone. Their mass spectra were found to be similar to those observed for other $RONO_2$, however, precise identification was not achieved.

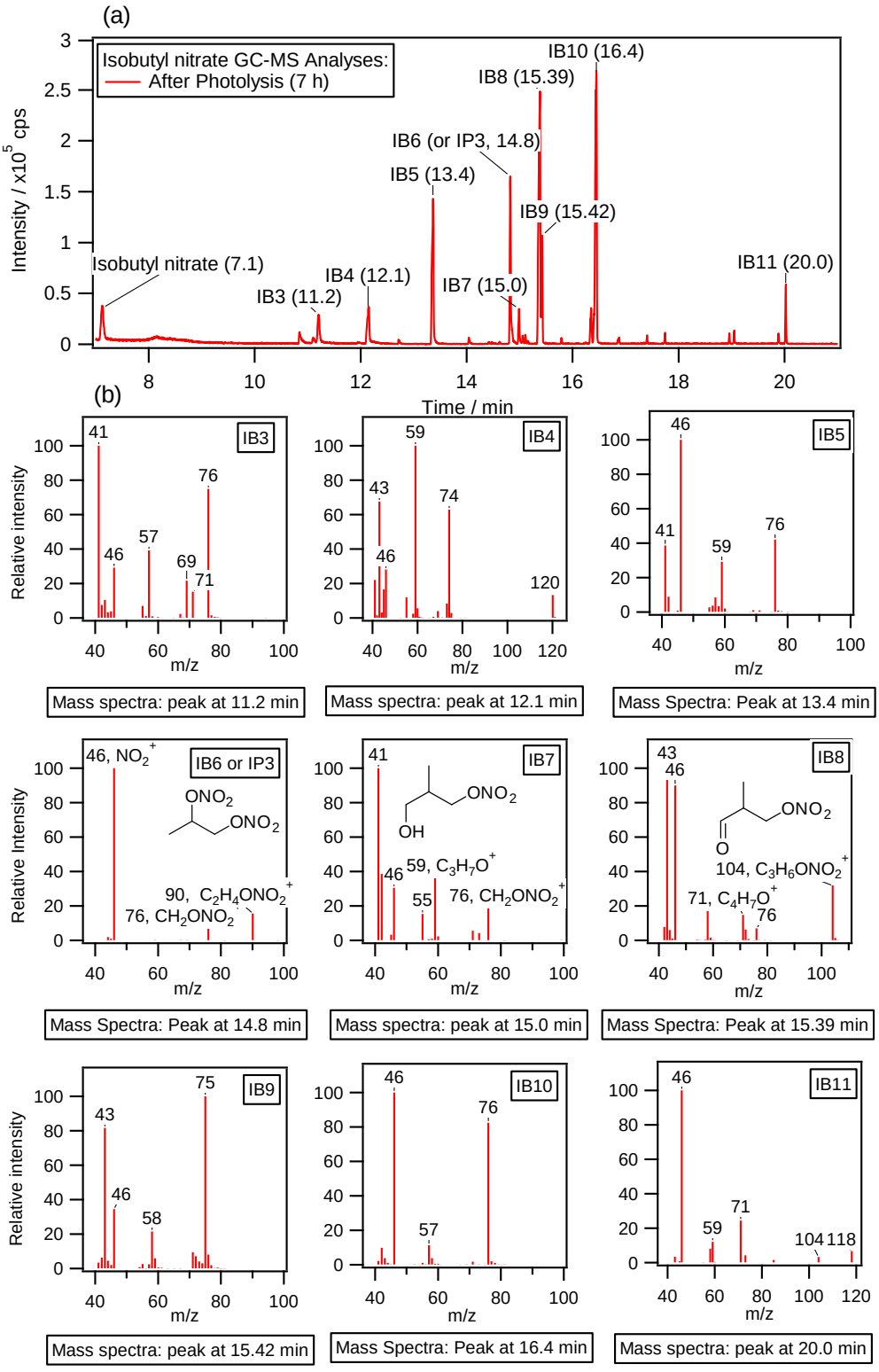

Figure S5.1: Isobutyl nitrate photolysis: (a) gas chromatogram (extracted for m/z = 46, NO_2^+) of the "end of reaction" of Exp. 7 in Table S1 (after 7 hours of photolysis) and (b) mass spectra for all detected peaks.

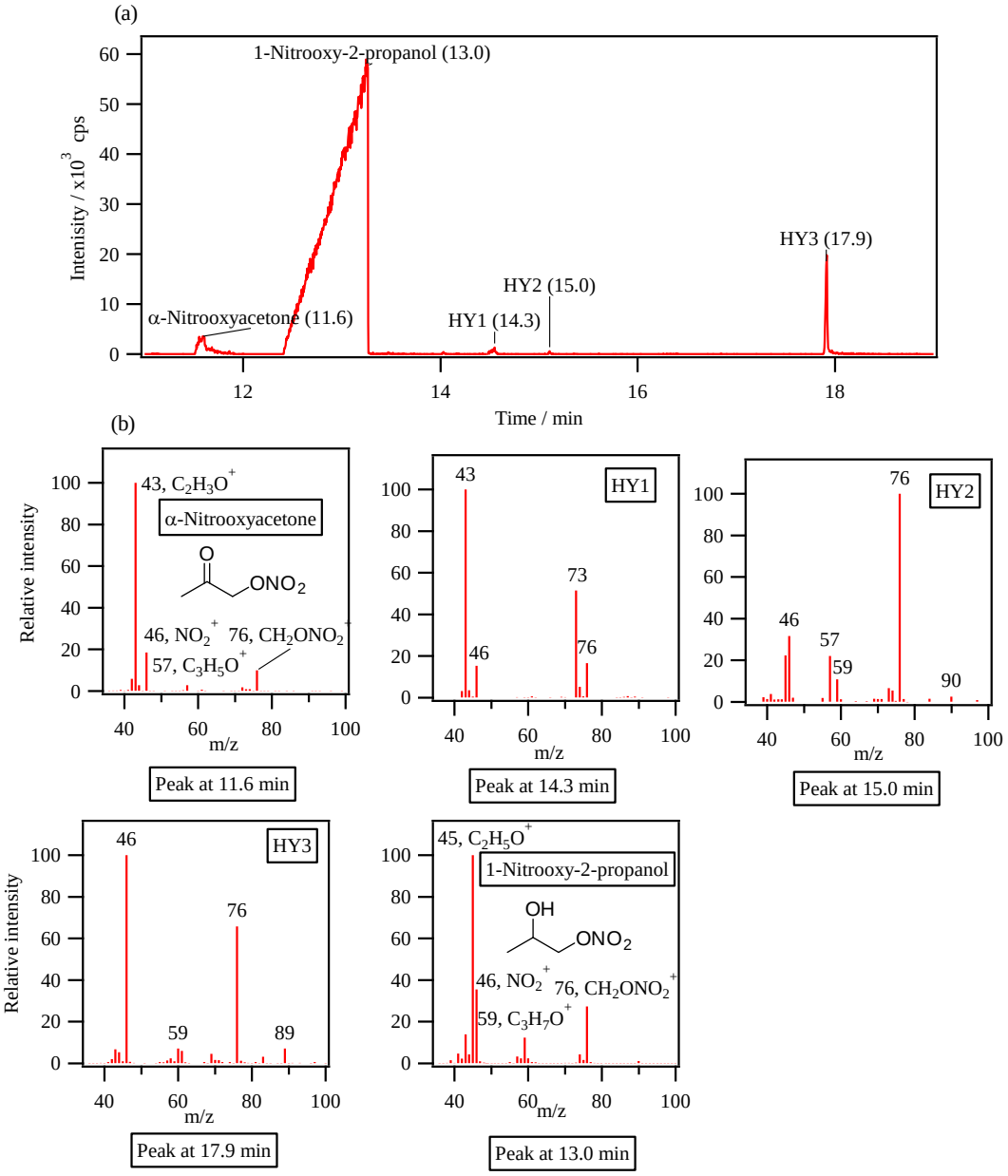

Figure S5.2: 1-Nitrooxy-2-propanol photolysis: (a) gas chromatogram of the "end of reaction" after 7 hours of photolysis (Exp 11 in Table 1) and (b) mass spectra of all detected peaks.

Section S6. Rejected hypothesis: ·NO2, (aq) direct formation followed by fast reactivity

$\cdot NO_2$ could be formed during the aqueous-phase photolysis of $RONO_2$ and then, transformed into HNO_2 and HNO_3 by hydrolysis through a reaction reported by Finlayson-Pitts and Pitts Jr., 2000:

$$2 \cdot NO_2 + H_2O \rightarrow HNO_2 + HNO_3 \quad \text{(RS1)}$$

with a reaction rate given by Eq. (S1):

$$\frac{-1}{2}\frac{d[\cdot NO_2]}{dt} = k_2[\cdot NO_2]^2 = \frac{d[HNO_2]}{dt} = \frac{d[HNO_3]}{dt} \qquad k_2 = 7 \cdot 10^7\ M^{-1}\ s^{-1} \quad \text{(S1)}$$

However, this reaction disagrees with our experiments where the formation of HNO_3 was exclusively observed as a secondary product (Fig. 2).

Another known pathway could be the aqueous-phase photolysis of $\cdot NO_{2(aq)}$ forming $\cdot NO_{(aq)}$.

$$\cdot NO_{2(aq)} + h\upsilon \rightarrow \cdot NO_{(aq)} + O(^3P), \quad \text{(RS2)}$$

followed by the reaction of $\cdot NO_{(aq)}$ with $\cdot NO_{2,(aq)}$ in solution, yielding two molecules of HNO_2 (Finlayson-Pitts and Pitts Jr., 2000).

$$\cdot NO + \cdot NO_2 + H_2O \rightarrow 2HNO_2\ , \quad \text{(RS3)}$$

with a reaction rate given by Eq. (S2):

$$\frac{-\cdot d[\cdot NO_2]}{dt} = k_3[NO][\cdot NO_2], \qquad k_3 = 3 \cdot 10^7\ M^{-1}\ s^{-1} \quad \text{(S2)}$$

This pathway is in better agreement with our observations of primary formation of HNO_2. Under this hypothesis, we calculated the steady-state concentrations of $\cdot NO_{2,(aq)}$, and $\cdot NO_{(aq)}$, and confronted the results with our experimental observations. To do so, we assumed that i) $RONO_2$ aqueous-phase photolysis yields 100 % $\cdot NO_{2,(aq)}$, and ii) $J_{\cdot NO_2(aq)} = \alpha \cdot J_{RONO_2(aq)}$ where $J_{RONO_2,(aq)} = 6 \cdot 10^{-6}\ s^{-1}$ (obtained for isopropyl nitrate from (González-Sánchez et al., 2023)) and α was varied from 10 to 6700 (which is the gas phase value, calculated from Clemitshaw et al., 1997; Madronich and Flocke, 1999; Roberts and Fajer, 1989; Talukdar et al., 1997 data). The steady-state concentrations of $\cdot NO_{2(aq)}$, and $\cdot NO_{(aq)}$ were derived from Eq. (S3) and Eq. (S4).

$$[\cdot NO_{2(aq)}] = \frac{-2\alpha J_{RONO_2} + \sqrt{(2\alpha J_{RONO_2})^2 + 8k_2 J_{RONO_2}[RONO_2]}}{4k_2} \quad \text{(S3)}$$

$$[\cdot NO_{(aq)}] = \frac{\alpha J_{RONO_2}}{k_3} \quad \text{(S4)}$$

Assuming α = 6700 and considering the initial $[RONO_2]$ of 1 mM, the aqueous-phase steady concentrations of $\cdot NO_{2(aq)}$ and $\cdot NO_{(aq)}$ were $6.3 \cdot 10^{-9}$ M and $1.3 \cdot 10^{-9}$ M, respectively. Considering their high volatilities ($K_H = 2.0 \cdot 10^{-2}$ and $1.8 \cdot 10^{-3}$ M atm^{-1}, respectively, Sander, 1999), and the volumes of the aqueous phase and the reactor's headspace (400 and 600 mL, respectively), around 310 and 740 ppb of $\cdot NO_{(g)}$ and $\cdot NO_{2(g)}$ would be observed in the reactor's headspace. Hence, both compounds should be detectable in our system by the NO_x analyzer. Even assuming a much lower α value of 10, concentrations of 330 ppb of $\cdot NO_{2(g)}$ would be observable. Under this scenario, one-fourth of this $\cdot NO_{2(g)}$ would be converted to ·NO through gas-phase photolysis.

Since no $\cdot NO_{2(g)}$ nor $\cdot NO_{(g)}$ were detected in the reactor's headspace during isopropyl nitrate photolysis (Fig. 1), hydrolysis of NO_x was thus rejected to explain the formation of HNO_2 and HNO_3 observed in our system.

Hydrolysis is not the only reaction that NO_x can undergo in the aqueous phase. Several studies have confirmed the nitration of aromatic compounds via $\cdot NO_2$ oxidation (Pang et al., 2019; Kroflič et al., 2015; Vione et al., 2003; Biswal et al., 2013; Vione et al., 2005, 2004). More appropriate to our system, Goldstein et al., (2004)

confirmed that $\cdot NO_2$ and $\cdot NO$ readily react with peroxy radicals ($ROO\cdot$) in the aqueous phase to form peroxynitrates ($ROONO_2$) and peroxynitrites (ROONO), respectively.

On the one hand, peroxynitrates are semi-stable molecules that present relatively long lifetimes in the aqueous phase. On the other hand, peroxynitrites are very short-lived compounds (lifetimes < 10^{-6} s) that can either decompose back to $RO\cdot$ and $\cdot NO_2$ or isomerize and form $RONO_2$. Due to the solvent cage effect, the yields of isomerization into $RONO_2$ are much enhanced compared to the gas phase reaction: around 84 – 89 % in the aqueous phase versus 1 – 35 % in the gas phase (Goldstein et al., 2004; Merényi et al., 2002; Atkinson et al., 1987).

However, even if the aqueous-phase photolysis of $RONO_2$ could directly form $\cdot NO_2$, no peroxy radicals could be directly formed in this system, preventing from any direct reaction $\cdot NO_2 + RO_2\cdot$. Therefore, this hypothesis was rejected.

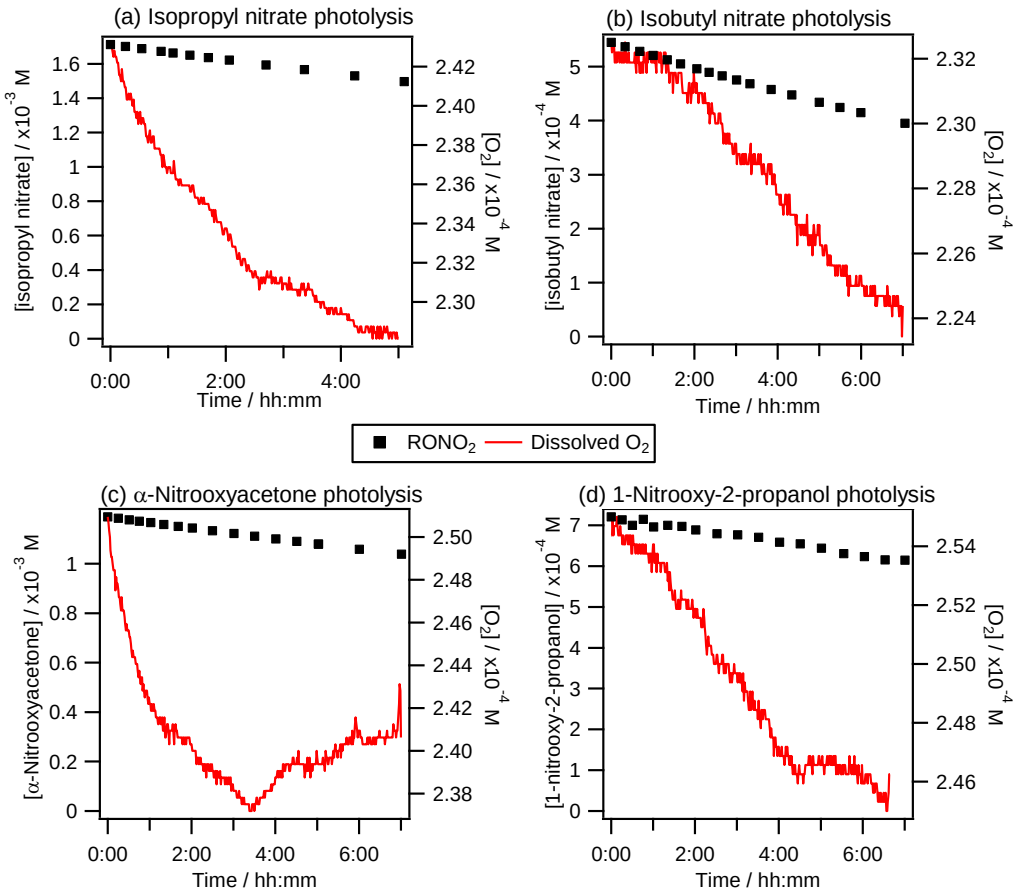

Figure S8: $RONO_2$ photolysis: time profiles of $RONO_2$ and the dissolved oxygen for (a) isopropyl nitrate (Exp. 2), (b) isobutyl nitrate (Exp. 8), (c) α-nitrooxyacetone (Exp. 10), and (d) 1-nitrooxy-2-propanol (Exp. 12).

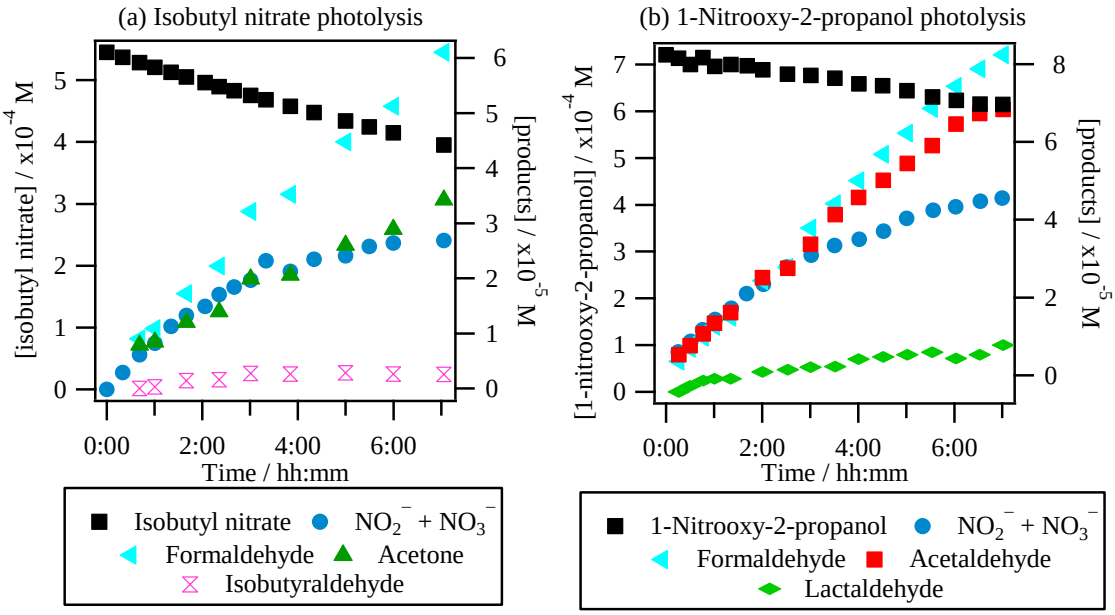

Figure S9: Primary carbonyl reaction products concomitant to HNO_2 + HNO_3 formation during photolysis of (a) isobutyl nitrate (Exp. 8) and (b) 1-nitrooxy-2-propanol (Exp. 11).

References

Atkinson, R., Aschmann, S. M., and Winer, A. M.: Alkyl nitrate formation from the reaction of a series of branched RO2 radicals with NO as a function of temperature and pressure, J Atmos Chem, 5, 91–102, https://doi.org/10.1007/BF00192505, 1987.

Biswal, J., Paul, J., Naik, D. B., Sarkar, S. K., and Sabharwal, S.: Radiolytic degradation of 4-nitrophenol in aqueous solutions: Pulse and steady state radiolysis study, Radiation Physics and Chemistry, 85, 161–166, https://doi.org/10.1016/j.radphyschem.2013.01.003, 2013.

Clemitshaw, K. C., Williams, J., Rattigan, O. V., Shallcross, D. E., Law, K. S., and Anthony Cox, R.: Gas-phase ultraviolet absorption cross-sections and atmospheric lifetimes of several C2-C5 alkyl nitrates, J Photochem Photobiol A Chem, 102, 117–126, https://doi.org/10.1016/S1010-6030(96)04458-9, 1997.

Finlayson-Pitts, B. J. and Pitts Jr., J. N.: Chemistry of the Upper and Lower Atmosphere, Academic P., Elsevier, https://doi.org/10.1016/b978-0-12-257060-5.x5000-x, 2000.

Goldstein, S., Lind, J., and Merenyi, G.: Reaction of Organic Peroxyl Radicals with˙NO2 and˙NO in Aqueous Solution: Intermediacy of Organic Peroxynitrate and Peroxynitrite Species, Journal of Physical Chemistry A, 108, 1719–1725, https://doi.org/10.1021/jp037431z, 2004.

González-Sánchez, J. M., Brun, N., Wu, J., Ravier, S., Clément, J.-L., and Monod, A.: On the importance of multiphase photolysis of organic nitrates on their global atmospheric removal, EGUsphere, 2023, 1–28, https://doi.org/10.5194/egusphere-2023-37, 2023.

Kroflič, A., Grilc, M., and Grgić, I.: Unraveling Pathways of Guaiacol Nitration in Atmospheric Waters: Nitrite, A Source of Reactive Nitronium Ion in the Atmosphere, Environ Sci Technol, 49, 9150–9158, https://doi.org/10.1021/acs.est.5b01811, 2015.

Madronich, S. and Flocke, S.: The Role of Solar Radiation in Atmospheric Chemistry, Springer, Berlin, Heidelberg, 1–26, https://doi.org/10.1007/978-3-540-69044-3_1, 1999.

Merényi, G., Lind, J., and Goldstein, S.: The rate of homolysis of adducts of peroxynitrite to the C=O double bond, J Am Chem Soc, 124, 40–48, https://doi.org/10.1021/ja011799x, 2002.

Pang, H., Zhang, Q., Lu, X., Li, K., Chen, H., Chen, J., Yang, X., Ma, Y., Ma, J., and Huang, C.: Nitrite-Mediated Photooxidation of Vanillin in the Atmospheric Aqueous Phase, Environ Sci Technol, 53, 14253–14263, https://doi.org/10.1021/acs.est.9b03649, 2019.

Roberts, J. M. and Fajer, R. W.: UV Absorption Cross Sections of Organic Nitrates of Potential Atmospheric Importance and Estimation of Atmospheric Lifetimes, Environ Sci Technol, 23, 945–951, https://doi.org/10.1021/es00066a003, 1989.

Ryerson, T. B., Williams, E. J., and Fehsenfeld, F. C.: An efficient photolysis system for fast-response NO2 measurements, Journal of Geophysical Research Atmospheres, 105, 26447–26461, https://doi.org/10.1029/2000JD900389, 2000.

Sander, R.: Compilation of Henry ' s Law Constants for Inorganic and Organic Species of Potential Importance in Environmental Chemistry, Database, 20, 107, https://doi.org/10.1017/CBO9781107415324.004, 1999.

Talukdar, R. K., Burkholder, J. B., Hunter, M., Gilles, M. K., Roberts, J. M., and Ravishankara, A. R.: Atmospheric fate of several alkyl nitrates: Part 2. UV absorption cross-sections and photodissociation

quantum yields, Journal of the Chemical Society - Faraday Transactions, 93, 2797–2805, https://doi.org/10.1039/a701781b, 1997.

Vione, D., Maurino, V., Minero, C., Vincenti, M., and Pelizzetti, E.: Aromatic photonitration in homogeneous and heterogeneous aqueous systems, Environmental Science and Pollution Research, 10, 321–324, https://doi.org/10.1065/espr2001.12.104.1, 2003.

Vione, D., Belmondo, S., and Carnino, L.: A kinetic study of phenol nitration and nitrosation with nitrous acid in the dark, Environ Chem Lett, 2, 135–139, https://doi.org/10.1007/s10311-004-0088-1, 2004.

Vione, D., Maurino, V., Minero, C., and Pelizzetti, E.: Nitration and photonitration of naphthalene in aqueous systems, Environ Sci Technol, 39, 1101–1110, https://doi.org/10.1021/es048855p, 2005.